The Effects of Low Molecular Weight Dicarboxylic Acids on Cloud Formation

Anthony J. Prenni,* Paul J. DeMott, Sonia M. Kreidenweis, and D. Eli Sherman

Department of Atmospheric Science, Colorado State University, Fort Collins, Colorado 80523-1371

Lynn M. Russell and Yi Ming

Department of Chemical Engineering, Princeton University, Princeton, New Jersey 08544

Received: June 26, 2001; In Final Form: September 25, 2001

The ubiquitous presence of organic compounds in tropospheric particles requires that their role in aerosol/cloud interactions be accounted for in climate models. In this paper, we present studies that investigate the hygroscopic behavior of organic compounds and their efficiency as ice nuclei. Specifically, results for soluble and partially soluble dicarboxylic acids that have been observed in atmospheric aerosol are discussed. At room temperature, we use a humidified tandem differential mobility analyzer (HTDMA) and a condensation particle counter interfaced with a cloud condensation nuclei counter to characterize the water uptake behavior of these acids. The HTDMA data agree quite well with modeled hygroscopic behavior. However, we find that some of the compounds retain water to very low humidities, never exhibiting efflorescence. The studies are extended to lower temperatures using a continuous flow ice thermal diffusion chamber to investigate the role of these species in ice nucleation at cirrus conditions. Results suggest that ice formation occurs via homogeneous nucleation for most of these acids, and that nucleation for these acids is not as efficient as that for sulfate aerosol.

Introduction

Atmospheric aerosols affect the earth's radiation budget directly by absorbing and scattering solar radiation and indirectly by serving as cloud condensation nuclei and ice nuclei. While background and sea salt aerosols are composed largely of inorganic species, a significant fraction of total fine particulate matter is composed of organics. For example, Chow[1] determined that 15−25% of fine particulate matter was typically organic in the Los Angeles Basin during the Southern California Air Quality Study, and White determined that organics usually constitute 20−50% of fine aerosol mass over the continental U.S.[2] Saxena et al.[3] showed that organics can alter the water uptake behavior of inorganic aerosol both positively and negatively and suggested that the hygroscopic behavior of soluble organics needs to be investigated in the laboratory. Organics may also constitute a significant fraction of atmospheric aerosol even at high altitudes,[4] which may be important for ice formation in clouds. Indeed, induced ice nucleation by monolayers of aliphatic alcohols has been reported.[5]

Rogge et al.[6] identified more than 80 organic compounds in atmospheric particles, including dicarboxylic acids. Dicarboxylic acids have also been identified in cloudwater samples collected at a high mountain range in central Europe,[7] in the condensed phase at a semi-urban site in the northeastern US,[8] in urban environments,[9,10] and in Arctic aerosol.[11] In these measurements, oxalic acid is often the most prevalent dicarboxylic acid, followed by malonic and succinic acids.

Low molecular weight dicarboxylic acids are produced in automobile exhaust, as emissions from meat cooking, and as emissions from pyrolysis of plants and other organic material.

* Corresponding author. Colorado State University, Department of Atmospheric Science, Fort Collins, CO 80523-1371. E-mail: tony@aerosol.atmos.colostate.edu. Phone: (970) 491 8414. Fax: (970) 491 8483.

TABLE 1: Dicarboxylic Acid Solubility and Vapor Pressure

compound	chemical formula	solubility in water[a] (mg/L) at 25 °C	vapor pressure (Torr)
oxalic acid	HOOC−COOH	2.2×10^5	3.5×10^{-5} [b]
malonic acid	HOOC−(CH_2)-COOH	7.6×10^5	1.0×10^{-5} [c]
succinic acid	HOOC−$(CH_2)_2$−COOH	8.3×10^4	6.9×10^{-7} [d]
glutaric acid	HOOC−$(CH_2)_3$−COOH	1.6×10^6	4.1×10^{-6} [c]
adipic acid	HOOC−$(CH_2)_4$−COOH	3.2×10^2	1.5×10^{-7} [d]

[a] *CRC Handbook of Physical Properties of Organic Chemicals.*[48] [b] Calculated for 30 °C from Table 3 in Makar.[17] [c] Calculated for 30 °C in Ribeiro da Silva et al.[14] [d] Calculated for 30 °C in Davies and Thomas.[15]

Photochemical reactions are also an important source of atmospheric dicarboxylic acids. For example, glutaric acid forms via the photooxidation of cyclohexene and cyclopentene.[12] Indeed, photooxidation is likely the dominant pathway to formation, as measured atmospheric concentrations of dicarboxylic acids in Los Angeles far surpassed contributions from direct emissions,[13] and seasonal trends suggest that dicarboxylic acids are largely produced in photochemical smog.[6,9]

Dicarboxylic acids have relatively low vapor pressures[14−17] and therefore are expected to partition to the condensed phase.[17] These acids are sufficiently soluble to be present in the water-soluble fraction of atmospheric particles.[18] Solubilities and vapor pressures are shown in Table 1. Yu[19] suggests that there is a need for accurate laboratory studies to determine the cloud condensation nuclei (CCN) activity of atmospherically relevant organic acids. Cruz and Pandis[20] showed that glutaric acid particles take up water above 85% RH and determined that glutaric acid and adipic acid act as efficient CCN.[21] Further, a glutaric acid coating on ammonium sulfate increased the CCN activity of ammonium sulfate aerosol,[22] as did coatings of other organic species.[23] Other laboratory studies indicate that highly

10.1021/jp012427d CCC: $20.00
Published on Web 11/21/2001

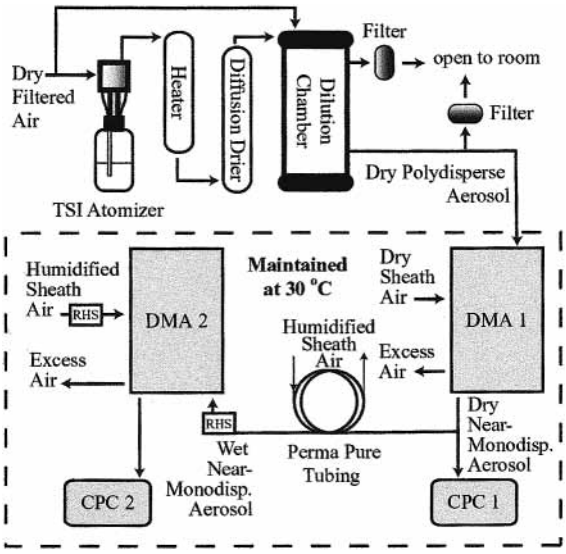

Figure 1. Schematic diagram of the humidified tandem differential mobility analyzer. RHS = relative humidity sensor.

soluble organic compounds have critical activation diameters near that of ammonium sulfate,[24] while the less soluble adipic acid has a significantly larger activation diameter. This suggests that the ability for an organic compound to act as an efficient CCN correlates with its solubility. Finally, field measurements indicate a strong correlation between CCN and oxalate concentrations,[25] suggesting that oxalate may play a role in activating CCN.

In this study, we investigate the hygroscopic growth and ice activation efficiency of five dicarboxylic acids: oxalic (ethanedioic) acid, malonic (propanedioic) acid, succinic (butanedioic) acid, glutaric (pentanedioic) acid, and adipic (hexanedioic) acid. The hygroscopic growth of submicrometer particles is investigated using a humidified tandem differential mobility analyzer at 30 °C and a condensation particle counter interfaced with a cloud condensation nuclei counter at room temperature, and ice formation behavior is investigated using a continuous flow ice thermal diffusion chamber at cirrus temperatures.

Experimental Section

Humidified Tandem Differential Mobility Analyzer. The humidified tandem differential mobility analyzer (HTDMA) has been used previously in our laboratory to measure the hygroscopic growth of submicrometer inorganic particles. It has been described fully[26] and will be described only briefly here. The apparatus is shown schematically in Figure 1. Polydisperse, submicrometer particles are generated from organic acid solutions using a TSI 3076 atomizer. The aerosol is then heated, dried, and diluted with dry air before entering the experimental chamber. For some studies, two heaters and two driers were employed to ensure complete drying. For all experiments, this drying procedure produced conditions of <5% relative humidity (RH) at 30 °C.

The experimental chamber, which includes everything described hereafter, is maintained at 30 °C. Prior to exposing the dry aerosol to humidified air, a size distribution is determined using the first differential mobility analyzer (DMA 1) and condensation particle counter (CPC 1) to ensure sufficient particle production. DMA 1 is operated at 15 LPM sheath flow and 1.5 LPM aerosol flow. The desired particle size is then selected using DMA 1, producing a near-monodisperse aerosol. For these studies, particle diameters of 100 and 50 nm were used. After size selection, the aerosol passes through the humidification system. Humidification is accomplished using Perma Pure tubing (model MD-110−48S), with the sheath flow operated at a desired humidity. Perma Pure tubing is impermeable to particles, but allows water vapor to be transported from the sheath flow to the aerosol. A size distribution is then taken of the 'wet' aerosol using the second DMA (DMA 2) and second particle counter (CPC 2). DMA 2 is operated with both flows humidified at 5 LPM sheath flow and 0.5 LPM aerosol flow. The DMA channel width for DMA 2 at 100 and 50 nm was 4.2 and 1.9 nm, respectively. For these studies, hygroscopic growth must therefore exceed ~4% of the dry particle diameter to be detected using the HTDMA.

For each compound, the first size distribution in DMA 2 was taken at 5% RH. For adipic acid, succinic acid, and oxalic acid measurements, the peak of the dry distribution fell near the desired size (50 or 100 nm). However, for glutaric acid and malonic acid, particle evaporation caused a decrease in particle diameter. For all compounds, the peak particle diameter measured at 5% RH is used as the "dry" particle diameter for hygroscopic growth calculations.

The near-monodisperse aerosol was then exposed to increasing relative humidity and particle diameter was monitored. The humidity at the inlet of DMA 2 was measured for both the aerosol sample flow and the sheath flow using ROTRONIC HydroClip humidity sensors (type S). Data are presented as a function of the aerosol flow RH. The measured RH for the sheath flow always fell within 2% of the RH for the sample flow. These sensors are accurate to ± 1.5% RH over the humidity range studied. The uncertainty of the sensors is pooled with the fluctuations in the humidity measurements to produce the errors bars in subsequent figures.

Organic-Electrolyte Thermodynamic Equilibrium Model. To compare the measured hygroscopic behavior to theoretically predicted growth, we have employed a semiempirical organic-electrolyte thermodynamic equilibrium model proposed by Ming and Russell.[27] This model uses group contribution method to describe the behavior of organic molecules in terms of their functional groups.[28] Empirical parameterizations were used to fit a large range of experimental data for alkanes, alcohols, ketones, carboxylic acids, and dicarboxylic acids with carbon chains of varying lengths. This approach allows predictions of the interactions of organic species in aqueous solutions with other organic components and with inorganic salts by a self-consistent incorporation of Pitzer interactions in the UNIFAC framework.[29,30] The model determines the free energy of a specified composition with varying amounts of condensed water in order to solve for the amount of water that will condense at a specified relative humidity.

This calculation predicts both the composition of the aerosol particle at equilibrium with a specified humidity and the free energy of that system. In the uptake of water by particles multiple equilibria exist in the hysteresis region of the hygroscopic growth curve. In this region, particles follow the lower (dry) branch as they deliquesce and then take up water, but as water evaporates with decreasing relative humidity they tend to follow an upper (wet) branch of equilibria until they reach the point at which they effloresce or crystallize.[31] Thus we have used the equilibrium model to predict the conditions under which metastable equilibria exist, providing descriptions of the expected behavior of both the deliquescence and efflorescence equilibrium branches. However, the model cannot be used to evaluate when metastable states form. In the case of the

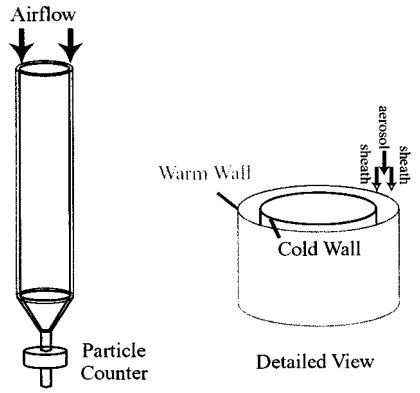

Figure 2. Schematic diagram of the continuous flow ice thermal diffusion chamber.

efflorescence branch, the point at which crystallization occurs is unknown and must be measured experimentally.

Cloud Condensation Nuclei Counter. A condensation particle counter (TSI 3025A) interfaced with a cloud condensation nuclei counter (modified Mee Industries, model 130) are used to investigate hygroscopic growth above water saturation. Particle generation and size selection are the same as for the HTDMA setup, with only 100 nm diameter particles being studied. The dry, size-selected aerosol flow is sent to the condensation particle counter (CPC), which measures condensation nuclei (CN) concentrations, and to the cloud condensation nuclei (CCN) counter. In the CCN counter, particles are exposed to humidities above water saturation, and laser light scattering from the aerosol is monitored using a CCD video camera. Prior to activation as cloud droplets, the particles are too small to be detected using the video camera. Upon activation, however, the particles grow to sizes which are large enough for detection. The number of activated particles is then determined from frame-by-frame analysis of the videotape and knowledge of the sample volume. Using this method, the ratio of CCN/CN can be determined for each compound over a range of water supersaturations.

Continuous Flow Ice Thermal Diffusion Chamber. The continuous flow ice thermal diffusion chamber (CFDC) has been used previously to measure ice formation from submicrometer particles,[32] and the experimental technique will be described only briefly here. Particle generation and size selection are the same as for the HTDMA setup, with 50 and 100 nm diameter particles studied. The dry aerosol is first sent through a precooler, operated at approximately −25 °C, which effectively removes any excess water vapor from the aerosol flow. The aerosol then enters the CFDC, shown schematically in Figure 2. The CFDC consists of an annular gap between two ice coated vertical cylinders. A laminar flow of aerosol passes through this annular space between two flows of dry, particle-free sheath air. The sheath flow constrains the aerosol to a region of well-defined temperature and humidity, which is determined by the temperatures of the ice-covered walls and the location of the aerosol sample. Wall temperatures are measured using an array of thermocouples placed along the length of the CFDC. The ice-coated walls are held at different temperatures, allowing for humidities well above ice saturation. The maximum ranges of RH and temperature across the lamina in these studies are 0.8% RH and 0.7 °C, respectively. Measurement precision is 0.6% RH and 0.7 °C.[32]

Upon nucleation of ice, particles grow rapidly as additional water vapor is transferred to the frozen particles. For a given experiment, relative humidity is incrementally increased at a given temperature, and particle size is monitored at the outlet of the CFDC using an optical particle counter (Climet 7350A). The optical particle counter detects particles greater than 0.4 μm in diameter. Upon reaching a size which is significantly larger than expected for hygroscopic growth at below water saturation, the aerosol is considered only to have been able to have formed ice. The cutoff diameter used in these studies is 1.3 micrometers. Particle growth is sufficiently fast that there is enough time for ice particles to grow to this size while in the CFDC. By knowing the number of particles introduced into the CFDC, and the number of ice particles formed, the percentage of particles that nucleate ice can be determined. Results are reported as a function of ice relative humidity. Specifically, we report the humidity at which ~1% of the particles form ice.

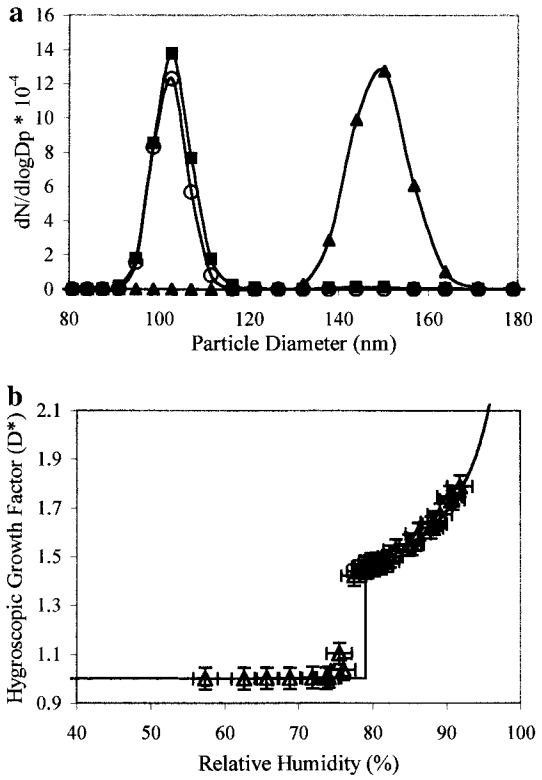

Figure 3. (a) Sample HTDMA data for ammonium sulfate aerosol at 30 °C. At 5% RH (open circles), the 100 nm aerosol sample is crystalline. As relative humidity is raised to 73% RH (solid squares), the aerosol remains crystalline and $D^* = 1$. Increasing the relative humidity slightly further, to greater than 77% RH (solid triangles), induces deliquescence, causing the aerosol to take up a significant amount of water such that $D^* = 1.46$. (b) HTDMA data for ammonium sulfate aerosol at 30 °C. A deliquescence transition is observable at 77.5% RH. Also shown as a solid line is the predicted ammonium sulfate deliquescence point[33] and the hygroscopic growth predicted using Köhler theory.

Results

Humidified Tandem Differential Mobility Analyzer. The hygroscopic growth factor D^* gives an indication of the amount of water absorbed by the particles and is calculated thusly: $D^* = D_{wet}/D_{dry}$, where D_{wet} is the diameter of the particle after being exposed to the enhanced humidity and D_{dry} is the dry droplet diameter, as determined from DMA 2 measurements at ≤5% RH. If the aerosol remains dry, the particles do not grow with increasing humidity, and $D^* = 1$. Upon reaching the deliquescence point, the particles take up water causing an increase in D^*. Ammonium sulfate was used to test the experimental setup because of its well-known deliquescence point. Figure 3a shows

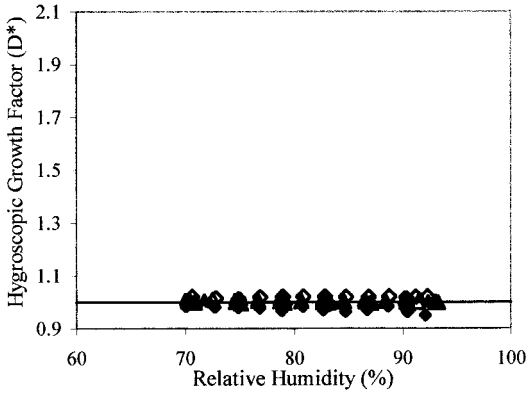

Figure 4. HTDMA data for 50 nm (solid triangles) and 100 nm (open triangles) diameter adipic acid, and 50 nm (solid diamonds) and 100 nm (open diamonds) diameter succinic acid particles. The particles do not undergo a deliquescence transition over the humidity range studied, and so $D^* = 1$. The solid line indicates no water uptake.

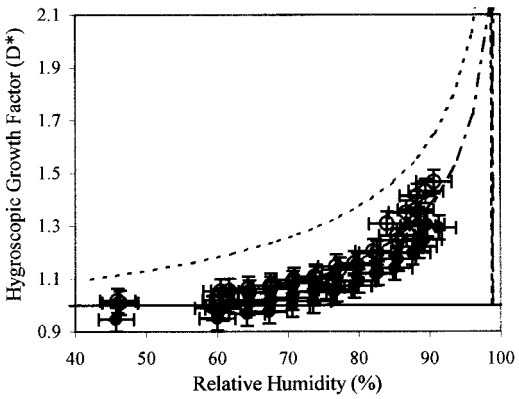

Figure 5. HTDMA data for 50 nm (solid circles) and 100 nm (open circles) diameter oxalic acid aerosol. Particle growth is evident above 60% RH. Also shown are predicted deliquescence points and the efflorescence branch of the growth curve for oxalic acid (dashed line) and oxalic acid dihydrate (dashed−dotted line), based on the organic-electrolyte model. The solid line indicates no water uptake.

an example of HTDMA data for ammonium sulfate before and after deliquescence. In the figure, the size distribution for the crystalline aerosol at 5% RH peaks near 100 nm. Relative humidity is increased to 73% RH, and no change is observed in particle diameter, indicating the aerosol remains crystalline. The small change in number density results from fluctuations in the atomizer output. Increasing the humidity slightly further to greater than 77% RH results in a large shift in particle size, indicating deliquescence. Our measured deliquescence relative humidity falls slightly below what has been recently measured for ammonium sulfate;[33,34] however, the data do agree with these previous measurements within the experimental uncertainty of the RH measurements. These data yield $D^* = 1.46$ for ammonium sulfate at ~77% RH. Hygroscopic growth measurements made over the range of 58−92% RH are shown in Figure 3b, along with the hygroscopic growth predicted using Köhler theory, with critical data as listed in DeMott et al.[35] and water activity from Clegg et al.[36] The figure shows good agreement between measurements and theory.

HTDMA studies were conducted for 50 and 100 nm diameter particles for adipic acid aerosol over the range of 70−93% RH and for succinic acid aerosol over the range of 70−92% RH. Results from these measurements are shown in Figure 4. For both of these compounds, D^* does not change as humidity is increased, indicating that their deliquescence points at 30 °C are outside of the humidity range studied. This agrees well with predictions from the semiempirical equilibrium model, which predicts a deliquescence point of approximately 99% RH for both compounds.

In the adipic acid and succinic acid studies, there was no clear evidence of water uptake below 93% relative humidity. Nonetheless, there was still some variability in the diameters measured by DMA 2. This variability is used as an indication of the uncertainty in our size measurements. On the basis of the assumption that particle diameter should not change over the humidity range studied for adipic acid and succinic acid, we determined that one standard deviation (σ) for D^* is 0.015. We used three standard deviations from these measurements as an indication of our uncertainty in D^* for oxalic acid, glutaric acid, and malonic acid measurements. This value corresponds well with the minimum growth that can be measured in our system, based on the channel width in DMA 2. Other factors may also contribute to the uncertainty in D^*. However, only this 3σ uncertainty is included in the figures.

Oxalic acid aerosol was studied in the HTDMA over the humidity range of 45−91% with 50 and 100 nm diameter particles. The thermodynamic model predicts a deliquescence relative humidity of 99% for oxalic acid particles, and so we do not expect to see water uptake over the humidity range studied. However, Figure 5 clearly shows oxalic acid particle growth with increasing relative humidity. This behavior could result if the particles did not effloresce when dried to <5% RH, so that the "dry" particles are actually concentrated solutions. A recent electrodynamic balance study indicated similar behavior for citric acid, glucose, and sorbitol, which also did not exhibit deliquescence or efflorescence behavior when exposed to varying humidities from 5 to 90% RH.[37] The hygroscopic behavior of the efflorescence branch of oxalic acid solution particles can be predicted using the model, as shown as a dashed line in Figure 5. The measured growth factors are significantly lower than the modeled behavior. One possible explanation is that liquid phase diffusion may be very slow in the concentrated, and possibly viscous, dicarboxylic acid solutions. If this is the case, all of the water may not have sufficient time to leave the particles during drying, causing the "dry" diameter used for the hygroscopic growth calculations to be in error. Furthermore, slow liquid-phase diffusion would not allow the equilibrium state to be reached when the humidity is increased during particle growth. Both effects would result in smaller hygroscopic growth factors than predicted by the model.

Data from Baxter and Lansing[38] indicate that below 5% RH oxalic acid will be anhydrous, but at and above 11% RH oxalic acid dihydrate will form. Therefore, modeling calculations are also presented in the efflorescence region for oxalic acid dihydrate. The similar deliquescence points for oxalic acid and oxalic acid dihydrate result from similar solubilities,[38,39] as well as from the fact that above 11% RH only the dihydrate is stable. Water uptake characteristics are also comparable, with a smaller growth factor predicted for the dihydrate. This results primarily from the difference in densities between the anhydrous and dihydrate forms. The efflorescence branch of the growth curve predicted by the model for oxalic acid dihydrate is shown as a dashed−dotted line in Figure 5, which agrees very well with our observations. Although these data indicate that oxalic acid dihydrate plays an important role in water uptake at room temperature, it is unclear if the dihydrate will be equally important at the lower temperatures used for the CFDC studies, discussed below.

Malonic acid aerosol was studied in the HTDMA over the humidity range of 50−93%. In contrast to the acids previously discussed, the particle size measured for malonic acid in DMA

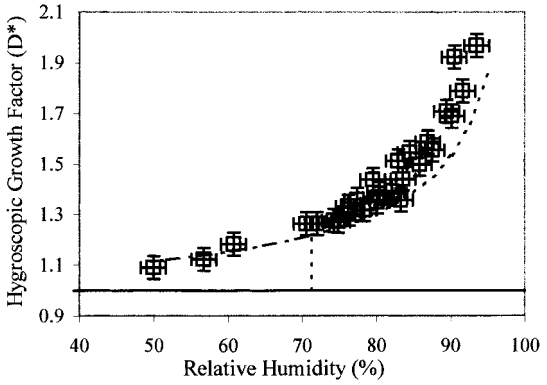

Figure 6. HTDMA data for 100 nm diameter malonic acid aerosol. Particle growth is evident throughout the humidity range studied. Also shown are the deliquescence point and water uptake curve (dashed line) predicted by the model, including the efflorescence branch of the growth curve (dashed−dotted line). The solid line indicates no water uptake.

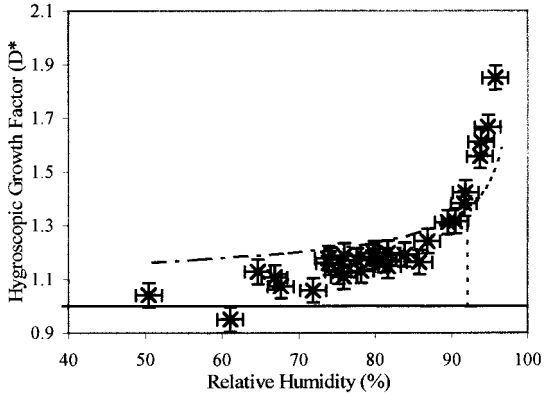

Figure 7. HTDMA data for 100 nm diameter glutaric acid aerosol. Particle growth is evident throughout the humidity range studied. Also shown is the deliquescence point and water uptake curve (dashed line) predicted by the model, including the efflorescence branch of the growth curve (dashed−dotted line). The solid line indicates no water uptake.

2 at 5% RH was not 100 nm, but rather ∼85 nm. As for all of the compounds, the measured particle size is used for growth calculations. This difference results because malonic acid partially evaporates after being size selected in DMA 1, but before reaching DMA 2. Dicarboxylic acids have relatively low vapor pressures. However, the vapor pressure of malonic acid is sufficiently high[14] that evaporation occurs upon dilution with dry air in the DMAs. Indeed, evaporation was such a large factor that neither HTDMA nor CFDC measurements could be taken for 50 nm particles, as much of the particle mass went into the gas phase. The vapor pressures for succinic acid and adipic acid are significantly lower,[15] such that evaporation was not a major factor. Oxalic acid, discussed previously, also has a high enough vapor pressure that some evaporation was expected, but it was not observed. This may have resulted due to the presence of oxalic acid dihydrate.

The semiempirical organic-electrolyte model predicts that malonic acid will deliquesce at 71% RH, significantly lower than any of the three previously discussed dicarboxylic acids. The data for malonic acid are shown in Figure 6, along with model calculations for 100 nm particles. The predicted behavior for 85 nm diameter particles is very similar to calculations for 100 nm diameter particles, so only results for 100 nm diameter particles are presented. The data indicate that the malonic acid particles did not exhibit a clear deliquescence transition, but rather gradual growth. As noted above, this behavior may result if the malonic acid aerosol retains water when initially dried to 5% RH. The efflorescence branch in the hysteresis region for hygroscopic growth and evaporation predicted by the model is shown as a dashed−dotted line. The data match the model well, suggesting that 5% RH is above the efflorescence point of malonic acid.

Glutaric acid has only a slightly lower vapor pressure than malonic acid, and again evaporation occurred. Semivolatile behavior of glutaric acid has also been reported in field measurements.[40] For this reason, hygroscopic growth factors were not obtained for 50 nm particles. For 100 nm particles, the semiempirical organic-electrolyte model predicts deliquescence at 92% RH. There is reasonable agreement between the measured values of D^* and the hygroscopic behavior predicted by the model, as shown in Figure 7. Once again, growth is evident at humidities below the deliquescence point. The relatively good agreement between the data and the model suggest that glutaric acid did not completely dry out at 5% RH, and so we place a limit of <5% RH on the glutaric acid efflorescence point. The poorer agreement at low RH's may again result from slow liquid-phase diffusion in the more concentrated particles. Significant growth is not evident until reaching humidities of greater than 85%. Cruz and Pandis[20] reported no water uptake by glutaric acid below 80% RH, and a hygroscopic growth factor of approximately 1.1 at 85% RH, indicating a deliquescence transition. This suggests that these authors were able to dry their particles sufficiently to crystallize glutaric acid prior to humidification. At higher humidities there is poor agreement between the current study and that of Cruz and Pandis,[20] as they did not report significant increases in D^* with increasing humidity. As noted, a major difference between these studies is that Cruz and Pandis were able to completely dry their particles, whereas we were not. Further, particle evaporation, which clearly has the potential to affect measured size distributions, was observed in both studies.

TABLE 2: Brief Summary of Results from HTDMA Studies for 100 nm Particles

compound	predicted deliquescence RH	observed deliquescence RH	D^* 80% RH	D^* 90% RH
oxalic acid	99%	efflorescence branch[a]	1.17	1.43
malonic acid	71%	efflorescence branch[a]	1.37	1.73
succinic acid	99%	no water uptake observed	1.01	1.01
glutaric acid	92%	efflorescence branch[a]	1.15	1.29
adipic acid	99%	no water uptake observed	1.00	1.00

[a] Indicates that water was associated with the particles below the deliquescence relative humidity and in the efflorescence branch of hygroscopic growth.

Data for all of the compounds are summarized in Table 2. In the table, measured hygroscopic growth factors are presented for each compound at 80% RH and 90% RH. Also given are the observed deliquescence behavior and the predicted deliquescence points of the compounds based on the thermodynamic model.

Cloud Condensation Nuclei Counter. CCN measurements were made for 100 nm diameter dicarboxylic acid particles at ∼20 °C. Data are presented as the fraction of particles which activate as cloud droplets, CCN/CN, as a function of water supersaturation SS_w (=RH − 100). Figure 8 shows CCN data for malonic acid particles, with a sigmoidal fit to the data shown as a solid line. The supersaturation at which 50% of the particles activate as cloud droplets, or CCN/CN = 0.5, is denoted with a dashed line. It is this value, $SS_{w50} = 0.24\%$ for malonic acid, which is taken as the measured critical supersaturation. It can be seen from the figure that the measurements were not carried

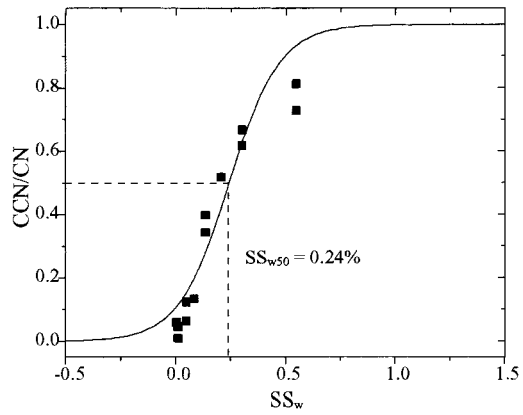

Figure 8. CCN data for 100 nm diameter malonic acid particles. The solid line is a sigmoidal fit to the data, which allows for determination of the supersaturation at which half of the particles have activated, SS_{w50}. For malonic acid, $SS_{w50} = 0.24\%$.

out to complete particle activation. This resulted due to an initial error in the calibration of the illuminated sample volume. This problem was corrected after the data were collected, and an accurate calibration was used to analyze the measurements. As a result, data were collected for CCN/CN ratios of 0.0 to 0.8. We do not believe that this affects our ability to accurately determine values for SS_{w50}.

The measured supersaturations can be compared to theoretical supersaturations for these compounds. Köhler theory predicts activation supersaturations based on two processes which affect the vapor pressure over a particle: the Kelvin effect, which increases vapor pressure due to the curvature of the particle, and the Raoult effect, which decreases vapor pressure due to the presence of soluble components. Upon reaching this critical supersaturation, the particles are expected to grow as long as this humidity is maintained. We used a simplified version of Köhler theory, as described fully in Cruz and Pandis,[21] to determine theoretical supersaturations. The simplified version of Köhler theory assumes that the solution is dilute, that the osmotic coefficient ≈ 1, and that solution surface tension and bulk density are equal to those of pure water. We used a value of 0.073 J m^{-2} for surface tension at 20 °C.[41] For these calculations, we must also assume a value for the average number of ions into which a solute molecule dissociates, ν. The dissociation constants for these compounds are relatively small, and so we assume $\nu = 1$. Of the compounds studied, oxalic acid has the largest dissociation constant, with a value of 5.9×10^{-2}, [41] from which we determined a slightly larger value of $\nu = 1.21$. Using this fractional value for ν_changes our theoretical supersaturation for oxalic acid from 0.20 to 0.18%. This small change in predicted supersaturation does not alter the interpretation of our results.

Values for experimental and theoretical supersaturations are tabulated in Table 3. There is good agreement between the theoretical and measured values for malonic acid, succinic acid, and glutaric acid, indicating that Köhler theory can be successfully applied to these relatively soluble organic compounds. These data can also be related to comparable studies which have investigated CCN activity of these compounds. However, in the related studies, dry particle diameter was incrementally increased while holding supersaturation constant, so a direct comparison cannot be made. For example, Cruz and Pandis[21] held supersaturation constant at 0.3% and determined an activation diameter of 111 nm for glutaric acid particles. This correlates well with our data for which 100 nm diameter glutaric acid particles activated at 0.32%. The slightly higher supersaturation

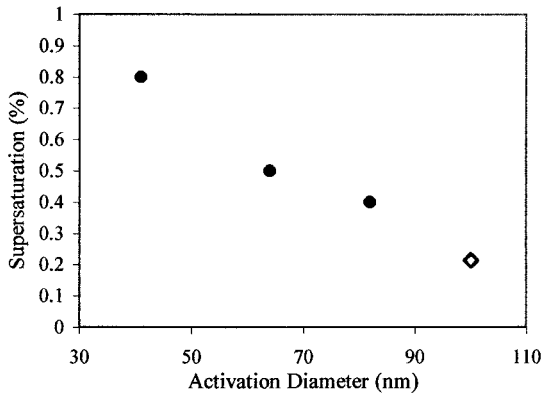

Figure 9. Succinic acid activation supersaturations as a function of particle diameter from this study (open diamond) and from the study by Corrigan and Novakov[24] (filled circles).

TABLE 3: CCN Activity for 100 nm Diameter Dicarboxylic Acids[a]

compound	theoretical critical supersaturation	measured critical supersaturation
oxalic acid	0.20%	0.44%
malonic acid	0.23%	0.24%
succinic acid	0.25%	0.21%
glutaric acid	0.28%	0.32%
adipic acid	0.30%	1.0%

[a] Data are for 20 °C. Parameters needed for calculations are taken from the *CRC Handbook*.[41]

from our study is expected, as we investigated smaller particles. For succinic acid, Corrigan and Novakov[24] determined activation diameters at three supersaturations. The supersaturations/diameters investigated in their study did not correspond well with the supersaturations/diameters investigated in our study. However, the trend in their data agrees well with ours, as shown in Figure 9.

The theoretical value of 0.20% for 100 nm diameter oxalic acid particles varies significantly from the experimentally determined supersaturation of 0.44%. As noted above, HTDMA data suggest that oxalic acid particles may retain a significant amount of water when dried to <5% RH. If so, the dry diameter used for the calculations here could be overestimated, resulting in a theoretical critical supersaturation which is lower than the observed critical supersaturation. However, this alone is not sufficient to fully account for the differences in the theoretical and measured values. Another factor may result in the time scale for particle growth. As noted above, liquid diffusion in the concentrated oxalic acid particles may be sufficiently slow that the particles may not activate as cloud droplets in the time frame of the experiment, further increasing the observed critical supersaturation. Oxalic acid may also convert to oxalic acid dihydrate. This conversion may be at least partially responsible for the disagreement. However, using parameters for oxalic acid dihydrate to calculate a theoretical supersaturation, we determined a theoretical critical supersaturation of 0.25%, still not in agreement with the experimentally determined value. It is unclear what other factors may play a role.

Our data suggest that a supersaturation of 1.0% must be reached for 100 nm adipic acid particles to activate. This disagrees greatly with our theoretical value of 0.30%. However, adipic acid is the least soluble of the compounds studied (see Table 1), and so it may diverge significantly from theoretical values expected for soluble particles. Our measured supersaturations are also significantly higher than previous measurements by Cruz and Pandis,[21] who determined an activation diameter

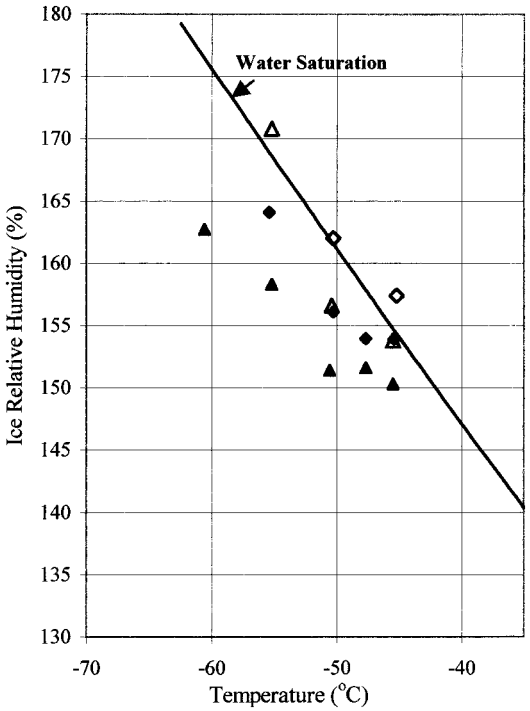

Figure 10. Ice nucleation data for 50 nm (diamonds) and 100 nm (triangles) diameter adipic acid aerosol. Data are presented for the humidity conditions in which 1% (solid symbols) and 10% (open symbols) of the particles formed ice. Also included are values for water saturation.

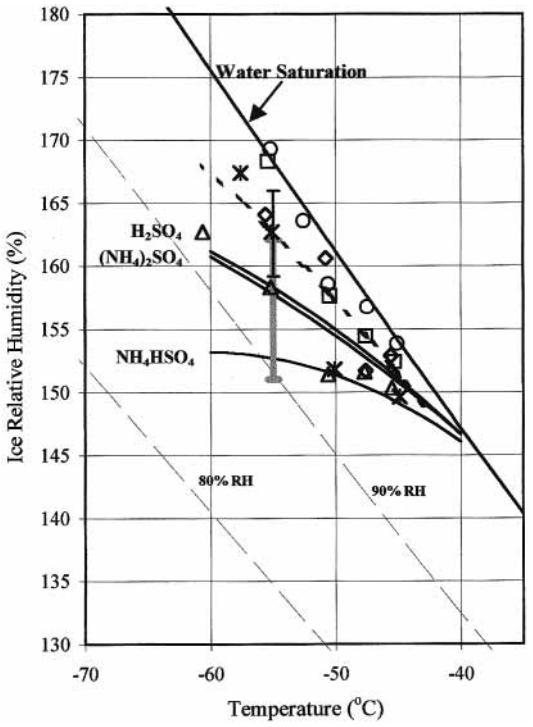

Figure 11. Ice nucleation data for 100 nm diameter adipic acid (open triangles), succinic acid (open diamonds), oxalic acid (open circles), glutaric acid (asterisks), and malonic acid (open squares) particles. Data are presented for the conditions in which 1% of the particles formed ice. The dashed line represents a polynomial fit to all of the dicarboxylic acid data. The black error bar indicates 1σ deviation from the fit. The gray error bar indicates 1σ uncertainty for sulfuric acid measurements. Also included are fits to data for 100 nm inorganic particles, as well as values for 80% RH, 90% RH, and water saturation.

of 115 nm for 0.3% supersaturation, and by Corrigan and Novakov,[24] who determined an activation diameter of 116 nm for 0.5% supersaturation. Despite these disagreements, data from our CFDC studies, discussed below, support the assertion that adipic acid may behave quite differently from the rest of the dicarboxylic acids, with less water uptake at high humidities.

Continuous Flow Ice Thermal Diffusion Chamber. Ice nucleation measurements were made for dicarboxylic acids over the temperature range of −45 to −60 °C using 50 and 100 nm diameter particles. In these studies, a near-monodisperse assembly of particles is introduced into the CFDC, and humidity is incrementally increased to well above ice saturation. Upon freezing, vapor transfer to the particles causes particle growth, which is observed using an optical particle counter. Freezing temperature results are presented as a function of relative humidity with respect to ice, RH_{ice}, where $RH_{ice} = (P_{chamber}/P_{ice}) \times 100$. $P_{chamber}$ is the vapor pressure in the aerosol lamina at the experimental temperature, and P_{ice} is the vapor pressure over ice at this same temperature.[42]

Data for ice nucleation from adipic acid aerosol are shown in Figure 10. Data are presented for both 50 and 100 nm particles and for 1% and 10% of the particle number frozen. From these data, several trends are apparent. First, higher ice relative humidity conditions are needed for freezing as temperature decreases, similar to trends seen for inorganic solution particles (e.g., refs 32 and 43). Second, freezing humidities for 50 nm particles are slightly higher than for 100 nm particles. This may result from a number of factors. If the particles deliquesce, they will take up water and grow, with higher humidities needed for dilution of 50 nm particles than for 100 nm particles due to the Kelvin effect. Further, homogeneous ice nucleation from solution particles is volume-dependent, with larger particles freezing more readily than smaller particles of the same composition. However, HTDMA studies at 30 °C suggest that very high humidities are needed for adipic acid deliquescence. If the particles remain crystalline, they may nucleate ice by serving as heterogeneous ice nuclei. In this case, ice nucleation may be surface-area-dependent or dependent on surface active sites, both of which favor ice nucleation of larger aerosol particles. Finally, not surprisingly, a higher humidity is needed to freeze 10% of the particles than 1% of the particles. For several of the acids at lower temperatures, the relative humidity needed to freeze 10% of the particles exceeds that for which convective stability is satisfied in the chamber at the flow rates chosen for these studies. Further, distinction between ice crystals and large, liquid-grown particles is more tenuous above water saturation. Because of these limitations, we focus on results for 1% of the particles frozen.

Figure 11 shows a summary of the freezing data for 100 nm particles. Included in the figure are fits to data collected previously in our laboratory for ice nucleation from 100 nm particles composed of sulfuric acid [H_2SO_4], ammonium sulfate [$(NH_4)_2SO_4$], and ammonium bisulfate [NH_4HSO_4] solution particles.[32] These inorganic particles constitute a large fraction of background aerosol in the upper troposphere and likely play a major role in cirrus formation. They therefore provide an important reference against which to compare the current results. Also included in the figure are values for 80% RH, 90% RH, and water saturation. At some point above water saturation, gas phase water is expected to condense on even relatively insoluble particles, producing particles that can rapidly freeze. The extent to which ice nucleation occurs below water saturation is thus an indication of the ability of the aerosol to induce cirrus formation.

For the 100 nm dicarboxylic acid particles, the acids exhibited relatively similar behavior for ice nucleation. This is surprising,

TABLE 4: Brief Summary of Results from CFDC Studies for 100 nm Particles

compound	ice saturation at −45 °c	ice saturation at −55 °c
oxalic acid	154%	169%
malonic acid	152%	168%
succinic acid	153%	164%
glutaric acid	150%	163%
adipic acid	150%	158%

as the compounds had very different water uptake characteristics at 30 °C, and so the composition of these compounds may be very different for a given humidity. For comparison, the ice saturation needed for freezing is given for each compound at two temperatures in Table 4. It can be seen that the least soluble adipic acid particles seem the most efficient at forming ice. This may result if the adipic acid particles nucleate ice by a mechanism different from the other acids. This is consistent with the CCN studies, which showed that 100 nm diameter adipic acid particles needed to reach 1.0% supersaturation before activating as cloud droplets at 20 °C. If adipic acid remains solid at low temperatures, ice nucleation may result from a heterogeneous process. Figure 11 shows that, in general, ice nucleation from organic aerosol is not as effective as ice nucleation from sulfate solution particles at −45 to −60 °C, particularly at the lower temperatures. This may result in part from a decreased efficiency in water uptake for some of the organic particles. For comparison, at 30 °C and 90% RH, the hygroscopic growth of ammonium sulfate is such that $D^* = 1.7$, while values for D^* for the dicarboxylic acids are generally lower (see Table 2).

A second-order polynomial is fit to the data to determine a relationship for ice formation humidity as a function of temperature for each of the acids studied. In all cases, a value of 2.1% RH_{ice} or less is determined for 1σ, and a value of 1.1% or less is determined for 1σ for 4 out of 5 of the acids. A second-order polynomial is also applied to the dicarboxylic acids, treating the acids as a group:

$$RH_{ice} = (-0.0093) \times \text{temp}(^\circ\text{C})^2 - (2.0494) \times \text{temp}(^\circ\text{C}) + 78.005$$

The fit is shown as a dashed line in Figure 11. Also shown is the value for 1σ for all of the data, 3.4% RH_{ice}, shown as a black error bar at −55 °C. For comparison, a gray error bar at −55 °C indicates an estimate of 1σ for H_2SO_4 measurements, based on fits to the freezing point depression parameter, λ.[32] While there is some overlap in the uncertainty in the measurements, the dicarboxylic acid fit is distinct from H_2SO_4. This difference is further evident when the relatively insoluble adipic acid is not included in the dicarboxylic acid fit. Koop et al.[44] suggest that ice nucleation depends strongly on solution activity, which may be applicable to our studies. Unfortunately, to our knowledge, low-temperature activity data do not exist for dicarboxylic acids, and so the data cannot be analyzed in this context. Previous studies have also related ice formation conditions to the parameter λ,[32,43,45] which relates the ice nucleation point depression in particles to the bulk melting point depression for solutions. However, as is the case for water activity, sufficient melting point depression data are not readily available for these compounds, and the ice nucleation point depression compared to equivalent-sized pure water particles cannot be computed due to the lack of water activity data, so such an analysis is not yet possible.

Ice nucleation conditions for 50 nm organic particles are shown in Figure 12. For comparison, fits to 50 nm inorganic solution data are also shown. Only data for adipic acid, succinic acid, and oxalic acid were collected, due to evaporation of the malonic acid and glutaric acid particles. The trends are similar to that for 100 nm particles, with nucleation occurring at somewhat higher relative humidities. The data show that oxalic acid and succinic acid are not effective at nucleating ice until reaching approximately water saturation, while adipic acid again stands out slightly as the most effective acid in forming ice. The size dependencies of nucleation may be partially responsible for the poor nucleating ability of these small particles. The Kelvin effect may also play a role, as higher humidities must be reached for dilution of these compounds than for their 100 nm counterparts.

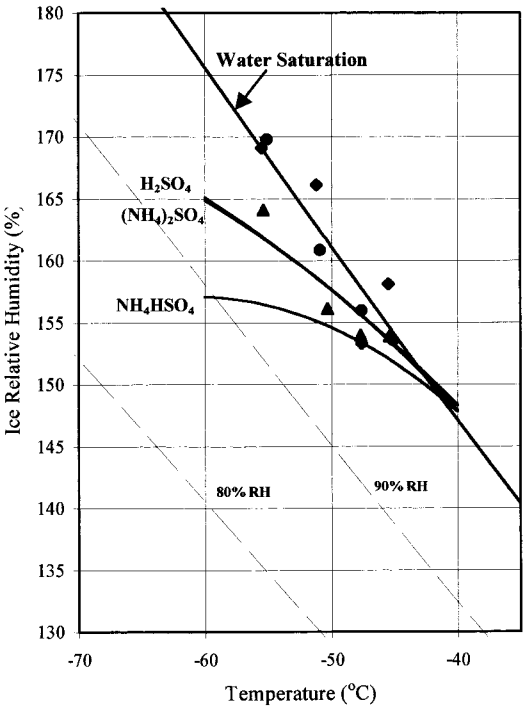

Figure 12. Ice nucleation data for 50 nm diameter adipic acid (solid triangles), succinic acid (solid diamonds), and oxalic acid (solid circles) particles. Data are presented for the conditions in which 1% of the particles formed ice. Also included are fits to data for 50 nm inorganic particles, as well as values for 80% RH, 90% RH, and water saturation.

Summary and Conclusions

The hygroscopic behavior of several dicarboxylic acids has been measured. The two least soluble samples studied, adipic acid and succinic acid, did not exhibit any water uptake up to 93% RH at 30 °C, consistent with the predicted deliquescence point of 99% RH. Adipic acid particles also did not readily activate as cloud droplets until reaching 1.0% supersaturation. Succinic acid particles, on the other hand, activated at 0.21% supersaturation. These data suggest that these compounds are not likely to exhibit hygroscopic growth under most humidity conditions, although they may play a role in developing haze particles after they have been processed by a cloud.

The remaining compounds, oxalic acid, malonic acid, and glutaric acid, each absorbed water at a lower relative humidity than the deliquescence relative humidity predicted by the model. These particles did not appear to effloresce during drying, even though they were dried to less than 5% RH. This suggests that once wetted in the atmosphere, these compounds are likely to remain as metastable solutions. For all three compounds, water uptake was similar to that for inorganic particles at high relative

humidities. Further, malonic acid and glutaric acid particles readily activated as cloud droplets at <0.3% supersaturation, while oxalic acid particles activated at a slightly higher supersaturation of 0.44%. Particles made of pure oxalic acid, malonic acid, or glutaric acid could thus play a role in haze formation and visibility reduction.

In the atmosphere, the dicarboxylic acids are likely to be internally mixed with an inorganic component. The presence of these acids may affect the inorganic particle's hygroscopic behavior. Indeed, Ansari and Pandis[30] calculated that the organic component may absorb a significant amount of water relative to the inorganic component at low relative humidities and high organic fractions. Further, Lightstone et al.[46] showed that the addition of succinic acid caused a slight decrease in the ammonium nitrate deliquescence point, and field studies have shown a strong positive correlation between oxalate concentrations and CCN in low altitude clouds.[25] Other dicarboxylic acids remain to be investigated.

HTDMA data at 30 °C suggest that oxalic acid, malonic acid, and glutaric acid all take up water readily at humidities greater than 90% RH, and so ice nucleation in these particles likely occurs from solution particles via homogeneous nucleation. Ice formation from succinic acid occurred under similar conditions, suggesting that ice nucleation in succinic acid occurs through a similar mechanism. However, ice nucleation from adipic acid particles occurred at slightly lower humidities. Adipic acid is the least soluble of the compounds studied and it did not activate as a cloud droplet until reaching significantly higher supersaturations than the other compounds, and so an alternative freezing mechanism is likely. In general, the organic acids had a humidity dependence similar to that for inorganic aerosol studied previously in our laboratory, although slightly higher humidities were needed to initiate freezing in the organics than for sulfate particles of comparable size. This decreased efficiency for ice nucleation may reflect differences in water activity between the organic and inorganic solution particles at low temperatures. These data suggest that in the upper troposphere aerosol rich in low molecular weight dicarboxylic acids could inhibit ice nucleation, allowing cirrus to form only at high humidities. There is some support from field measurements[47] that cirrus sometimes form at greater humidities than expected for pure sulfates.

These studies provide some of the first data for ice nucleation from organic solution particles and provide insight into possible cloud formation activity of organic aerosol. In the atmosphere, however, organics will likely be in the form of mixed inorganic/organic particles. Studies investigating the water uptake and ice activity of such mixed particles are thus needed.

Acknowledgment. This research was supported by the NOAA Postdoctoral Program in Climate and Global Change, administered by the University Corporation for Atmospheric Research. This material is based upon work supported by the National Science Foundation under Grant ATM 0071321.

References and Notes

(1) Chow, J. C.; Watson, J. G.; Fujita, E. M.; Lu, Z.; Lawson, D. R.; Ashbaugh, L. L. *Atmos. Environ.* **1994**, *28*, 2061−2080.

(2) White, W. Contributions to Light Scattering. In *Visibility: Existing and Historical Conditions: Causes and Effects*; Acidic Deposition State Science Report 24, Section 4; National Acid Precipitation Assessment Program: Washington, DC, 1990; pp 24-85−24-102.

(3) Saxena, P.; Hildemann, L. M.; McMurry, P. H.; Seinfeld, J. H. *J. Geophys. Res.* **1995**, *100*, 18,755−18,770.

(4) Murphy, D. M.; Thomson, D. S.; Mahoney, M. J. *Science* **1998**, *282*, 1664−1669.

(5) Popovitz-Biro, R.; Wang, J. L.; Majewski, J.; Shavit, E.; Leiserowitz, L.; Lahav, M. *J. Am. Chem. Soc.* **1994**, *116*, 1179−1191.

(6) Rogge, W. F.; Mazurek, M. A.; Hildemann, L. M.; Cass, G. R.; Simoneit, B. R. T. *Atmos. Environ.* **1993**, *27A*, 1309−1330.

(7) Puxbaum, H.; Limbeck, A. Scavenging of Organic Aerosol Constituents in Supercooled Clouds. Presented at the 13th International Conference on Clouds and Precipitation, Reno, NV, 2000.

(8) Khwaja, H. A. *Atmos. Environ.* **1995**, *29*, 127−139.

(9) Kawamura, K.; Ikushima, K. *Envir. Sci. Technol.* **1993**, *27*, 2227−2235.

(10) Kawamura, K.; Kaplan, I. R. *Envir. Sci. Technol.* **1987**, *21*, 105−110.

(11) Kawamura, K.; Kasukabe, H.; Barrie, L. A. *Atmos. Environ.* **1996**, *30*, 1709−1722.

(12) Grosjean, D.; Cauwenberghe, K. V.; Schmid, J. P.; Kelley, P. E.; James N. Pitts, J. *Environ. Sci. Technol.* **1978**, *12*, 313−317.

(13) Rogge, W. F.; Hildemann, L. M.; Mazurek, M. A.; Cass, G. R.; Simoneit, B. R. T. *J. Geophys. Res.* **1996**, *101*, 19379−19394.

(14) Silva, M. A. V. R. d.; Monte, M. J. S.; Ribeiro, J. R. *J. Chem. Thermodyn.* **1999**, *31*, 1093−1107.

(15) Davies, M.; Thomas, G. H. *Trans. Faraday Soc.* **1960**, *56*, 185−192.

(16) Bradley, R. S.; Cotson, S. *J. Chem. Soc.* **1953**, 1684−1688.

(17) Makar, P. A. *Atmos. Environ.* **2001**, *35*, 961−974.

(18) Saxena, P.; Hildemann, L. M. *J. Atmos. Chem.* **1996**, *24*, 57−109.

(19) Yu, S. *Atmos. Res.* **2000**, *53*, 185−217.

(20) Cruz, C. N.; Pandis, S. N. *Envir. Sci. Technol.* **2000**, *34*, 4313−4319.

(21) Cruz, C. N.; Pandis, S. N. *Atmos. Environ.* **1997**, *31*, 2205−2214.

(22) Cruz, C. N.; Pandis, S. N. *J. Geophys. Res.* **1998**, *103*, 13,111−13,123.

(23) Gorbunov, B.; Hamilton, R.; Clegg, N.; Toumi, R. *Atmos. Res.* **1998**, *48*, 271−283.

(24) Corrigan, C. E.; Novakov, T. *Atmos. Environ.* **1999**, *33*, 2661−2668.

(25) Liu, P. S. K.; Leaitch, W. R.; Banic, C. M.; Li, S.-M.; Ngo, D.; Megaw, W. J. *J. Geophys. Res.* **1996**, *101*, 28,971−28,990.

(26) Brechtel, F. J.; Kreidenweis, S. M. *J. Atmos. Sci.* **2000**, *57*, 1872−1887.

(27) Ming, Y.; Russell, L. M. *A.I.Ch.E. J.* **2001**. Submitted for publication.

(28) Reid, R. C.; Prausnitz, J. M.; Poling, B. E. *The Properties of Gases and Liquids*; McGraw-Hill: Boston, 1987.

(29) Clegg, S. L.; Seinfeld, J. H.; Brimblecombe, P. *J. Aerosol Sci.* **2001**, *32*, 713−738.

(30) Ansari, A. S.; Pandis, S. N. *Envir. Sci. Technol.* **2000**, *34*, 71−77.

(31) Tang, I. N.; H. R.Munkelwitz; Wang, N. *J. Colloid Interface Sci.* **1986**, *114*, 409−415.

(32) Chen, Y.; DeMott, P. J.; Kreidenweis, S. M.; Rogers, D. C.; Sherman, D. E. *J. Atmos. Sci.* **2000**, *57*, 3752−3766.

(33) Onasch, T. B.; Siefert, R. L.; Brooks, S. D.; Prenni, A. J.; Murray, B.; Wilson, M. A.; Tolbert, M. A. *J. Geophys. Res.* **1999**, *104*, 21,317−21,326.

(34) Cziczo, D. J.; Nowak, J. B.; Hu, J. H.; Abbatt, J. P. D. *J. Geophys. Res.* **1997**, *102*, 18,843−18,850.

(35) DeMott, P. J.; Meyers, M. P.; Cotton, W. R. *J. Atmos. Sci.* **1994**, *51*, 77−90.

(36) Clegg, S. L.; Brimblecomb, P.; Wexler, A. *J. Phys. Chem. A* **1998**, *102*, 2137−2154.

(37) Peng, C.; Chow, A. H. L.; Chan, C. K. *Aerosol. Sci. Technol.* **2001**, *35*, 753−758.

(38) Baxter, G. P.; Lansing, J. E. *J. Am. Chem. Soc.* **1920**, *42*, 419.

(39) Hill, L. M.; Goulden, T. P.; Hatton, E. *J. Chem. Soc.* **1946**, 78−81.

(40) Limbeck, A.; Puxbaum, H.; Otter, L.; Scholes, M. C. *Atmos. Environ.* **2001**, *35*, 1853−1862.

(41) Weast, R. C., Astle, M. J., Eds. *CRC Handbook of Chemistry and Physics*; 61st ed.; CRC Press: Boca Raton, 1981.

(42) Buck, A. L. *J. Appl. Meteorol.* **1981**, *20*, 1527−1532.

(43) Prenni, A. J.; Wise, M. E.; Brooks, S. D.; Tolbert, M. A. *J. Geophys. Res.* **2001**, *106*, 3037−3044.

(44) Koop, T.; Luo, B.; Tsias, A.; Peter, T. *Nature* **2000**, *406*, 611−614.

(45) Rasmussen, D. H. *J. Cryst. Growth* **1982**, *56*, 56−66.

(46) Lightstone, J. M.; Onasch, T. B.; Imre, D.; Oatis, S. *J. Phys. Chem. A* **2000**, *104*, 9337−9346.

(47) Heymsfield, A. J.; Miloshevich, L. M.; Twohy, C.; Sachse, G.; Oltmans, S. *Geophys. Res. Lett.* **1998**, *25*, 1343−1346.

(48) Howard, P. H., Meylan, W. M., Eds. *CRC Handbook of Physical Properties of Organic Chemicals*; CRC Press: Boca Raton, 1997.